JOURNAL OF MATERIALS SCIENCE 30 (1995) 3061–3074

An improvement in processing of hydroxyapatite ceramics

M. G. S. MURRAY*, J. WANG‡, C. B. PONTON*‡, P. M. MARQUIS*‡§
School of Metallurgy and Materials, ‡IRC in Materials for High Performance Applications, and §Biomaterials, School of Dentistry, The University of Birmingham, Edgbaston, Birmingham, B15 2TT, UK

Hydroxyapatite ceramics have been fabricated via two different processing routes, a conventional processing route and an emulsion-refined route. The conventional precipitation processing of powder precursors for hydroxyapatite ceramics results in the formation of hard particle agglomerates, which degrade both the compaction and densification behaviour of the resultant powder compacts. An emulsion-refinement step has been shown to be effective in "softening" particle agglomerates present in the conventionally processed powder precursor. As a result, the emulsion-refined powder compact exhibits both a higher green density and a higher sintered density than the un-refined powder compact, on sintering at temperatures above 800 °C. The effect of powder agglomeration on densification during both the initial and later stage of sintering is discussed. The attainable sintered density of the conventionally processed material was found to be limited by the presence of hard powder agglomerates, which were not effectively eliminated by the application of a pressing pressure of 200 MPa. These hard powder agglomerates, which form highly densified regions in the sintered ceramic body, commenced densification at around 400 °C which is more than 100 °C lower than the densification onset temperature for the emulsion-refined powder compact, when heated at a rate of 5 °C min^{-1}. The inter-agglomerate voids, manifested by the differential sintering, resulted in the formation of large, crack-like pores, which act as the strength-limiting microstructural defects in the conventionally processed hydroxyapatite. A fracture strength of 170 ± 12.3 MPa was measured for the emulsion-refined material compared to 70 ± 15.4 MPa for the conventionally processed material, when both were sintered at 1100 °C for 2 h.

1. Introduction

Hydroxyapatite (HA), which is the major mineral constituent of natural teeth and bone, is regarded as an important implant material with significant clinical potential [1]. Current clinical applications for this material are principally as bone substitutes or as coatings on prostheses. Synthetic hydroxyapatite precursors are produced via a variety of ceramic processing routes, including precipitation, sol–gel routes and hydrothermal processing routes [2–4]. Unfortunately, many of these processing techniques lack inherently clear approaches to exercising control over the development of microstructural heterogeneities and promoting microstructural uniformity when the precursors are fired at the sintering temperature. Conventional processing routes also often lead to the formation of hard particle agglomerates, which in the as-prepared powder precursors exhibit a higher green density than the surrounding matrix [5, 6]. It is almost impossible to eliminate these hard agglomerates using conventional compaction techniques, such as die-pressing and isostatic pressing. The presence of agglomerates in ceramic powder compacts results in the occurrence of differential sintering at the sintering temperature and the formation of strength-limiting microstructural flaws in the sintered ceramics [7]. The existence of processing-related microstructural defects and the resultant low strength restricts hydroxyapatite to being used only in non-load-bearing applications. An improvement in processing technology could, therefore, extend the application of hydroxyapatite to a higher load-bearing range where certain mechanical properties, such as fracture strength and fracture toughness, are required.

In order to refine the microstructure and improve the mechanical properties of a sintered hydroxyapatite ceramic, approaches have been taken to control the quality of precursor materials through parameters such as particle size, shape and distribution, and the degree of particle agglomeration [8]. An agglomerate-free ultrafine powder precursor, which exhibits a high surface area and therefore high sinterability, will lead to a lowered sintering temperature combined with small and uniform grain-size distribution in the

0022–2461

sintered ceramic. Several chemical-based processing routes have proved to be attractive in refining precursor characteristics for hydroxyapatite ceramics. Notably, Roy [9] and Hardy *et al.* [10] prepared hydroxyapatite powder precursors via sol–gel processing routes using metal alkoxides as the starting materials. Unfortunately, the powder precursors prepared by these authors exhibited a low sinterability, due to the formation of hard agglomerates, although the individual crystallite sizes were fine. The high processing costs for a large-scale production via these chemically based processing routes may also limit their application for preparing hydroxyapatite ceramics.

The alternative is to fabricate hydroxyapatite ceramics with well-controlled microstructure and improved mechanical properties by modifying certain well-established conventional processing routes. One of these alternative approaches is the use of emulsion technology, which has been studied extensively over the past 25 years [11]. The potential of emulsion techniques as a refinement measure for preparing fine and agglomeration-free ceramic powders has recently been realized. Reyen *et al.* [12] investigated the emulsion approach for preparing a wide variety of ceramic powders, and Celikkaya and Akinc [13], Kanai *et al.* [14], Ramamurthi *et al.* [15] and Maher *et al.* [16] have performed experiments with a variety of emulsion techniques. During the emulsion refinement, any reaction and crystallization take place in a very limited volume domain provided by the droplets. The microemulsions, each of which may be regarded as a microreactor, refine the clustering and subsequent crystallization and grain growth which occur in ceramic powder precursors during the drying and calcination stages. The objective of the present work was to study the effect of introducing an emulsion-conditioning stage [17] on the characteristics of a hydroxyapatite powder precursor and on the subsequent densification and microstructural development of the powder compact at the sintering temperature. The effect of powder agglomeration on densification at the sintering temperature and the resultant microstructure of the sintered ceramic will be discussed, together with the mechanical properties measured on the material.

2. Experimental procedure

Powder precursors for sintered hydroxyapatite ceramics were manufactured via two processing routes: (i) conventional processing route (CP), and (ii) emulsion-refinement route (ER). The conventional processing involved the initial formation of an appropriate amount of 0.5 M calcium hydroxide suspension, using calcium hydroxide powder (Analar grade, BDH Chemicals Ltd, UK) as the starting material. The suspension was vigorously stirred at 2000 r.p.m. whilst adding 0.3 M orthophosphoric acid solution (Analar grade, BDH Chemicals Ltd, UK). The orthophosphoric acid solution was added at a drip rate of 1–2 drops per second whilst controlling the pH (pH < 7) and temperature (25 °C) of the suspension to form a gelatinous precipitate [18]. Once the precipitate had been stirred and aged for 72 h, it was dried at 50 °C for 18 h. The as-dried powder precursor was ground in a mortar and pestle to eliminate large powder lumps.

For the emulsion refinement, an oil-in-water (O/W) emulsion system was first prepared, by mixing a given amount of distilled water together with appropriate amounts of cosurfactant ethanol (BDH Chemicals Ltd, UK), non-ionic surfactant (Triton X-100, BDH Chemicals Ltd, UK) and pure vegetable oil. The mixture was further homogenized in an ultrasonic bath (240 V, Ultrasonic Ltd, UK) to produce a stable emulsion. Excess oil was removed using a separating funnel, leaving only the O/W emulsion. A second batch of the gelatinous calcium phosphate was prepared as detailed above. The oil-in-water emulsion solution was then added to the gelatinous solution at a controlled rate whilst being ultrasonically agitated. The resulting sol was then centrifuged for 5 min at 2000 r.p.m. in order to remove any excess emulsion phases and to form a hydroxyapatite precursor gel. This was then subsequently dried at 50 °C for 18 h. Both the conventionally processed and emulsion-refined powders were further ground and characterized for phases present and surface characteristics using X-ray diffraction (XRD, CuK_α) and Fourier transform–infrared spectroscopy (FT–IR), respectively. Simultaneous thermogravimetry (TG) and differential thermal analyses (DTA) at a heating rate of 10 °C min^{-1} in air were carried out on both powder precursors (Type 780, Stanton Redcroft STA, UK).

Two types of powder compacts were prepared for both the CP and ER powders by uniaxially cold pressing 0.5 and 1.15 g powder in 10 and 24 mm diameter dies at a 15 and 40 MPa pressing pressure, respectively. The former, which were for the dilatometry study, exhibited dimensions of 10 mm (diameter) × 7.2 mm (height) and 10 mm (diameter) × 6.4 mm (height) for the conventionally processed and the emulsion-refined powders, respectively. The 24 mm diameter pellets exhibited a thickness of 2.4 and 2.1 mm and a compacted green density of 33.3% and 38.7% theoretical density (density of hydroxyapatite 3.156 g cm^{-3}) for the conventionally processed and the emulsion-refined powders, respectively, as measured on the basis of pellet mass and dimensions. The dilatometry study was carried out in air at a heating rate of 5 °C min^{-1} from room temperature up to 1100 °C in a tube furnace (Stanton Ltd, UK). The 24 mm diameter powder compacts were sintered in air in an electric furnace for 2 h at 800, 900, 1000, 1100 and 1200 °C, respectively. Each sample was heated from room temperature to 800 °C at a heating rate of 2 °C min^{-1} and kept at this temperature for 3 h before being heated to the desired sintering temperature at a rate of 2 °C min^{-1}. On completion of sintering at each sintering temperature, the sintered materials were cooled from the sintering temperature to room temperature at a rate of 5 °C min^{-1}.

The sintered pellets were characterized for sintering shrinkage and sintered density. For those sintered at temperatures below 1000 °C, density measurements were made on the basis of specimen mass and

dimensions. For those sintered at temperatures above 1000 °C, where the open porosity level was low, density was measured using the Archimedes' method in distilled water. Microstructural characterization using SEM was performed on both the fractured and polished surfaces of the sintered hydroxyapatite at each sintering temperature. Average fracture strengths of the sintered materials, which exhibited a diameter in the range of 16.6–16.7 mm and a thickness in the range of 1.2–1.5 mm, were determined using a standard shell test [19]. At least 15 tests were made for each material.

3. Results and discussion

3.1. Phase development

As shown in Fig. 1a and b, the emulsion refinement did not result in any significant change in phases present in both the as-dried powder precursor (50 °C for 12 h) and sintered material (1100 °C for 2 h) when compared with the conventionally processed powder precursor and sintered hydroxyapatite. The peak broadening in the as-dried powder precursors indicates the presence of a certain amount of amorphous or nanoscale sized phases. Crystalline hydroxyapatite and small amounts of β-tri-calcium phosphate and calcium oxide developed in both powder precursors on sintering at 1100 °C for 2 h. However, the diffraction peaks for β-tri-calcium phosphate and calcium oxide in the material prepared from the emulsion-refined powder precursor (ER) are weaker than those in the material prepared from the un-refined powder precursor. This indicates that the former is a more stoichiometrically homogeneous hydroxyapatite than the latter (CP).

The emulsion refinement involved oil, which was believed to result in the presence of organic residuals in the as-dried ER powder precursor. Fig. 2a and b are FT–IR spectra for the conventionally processed and emulsion-refined powder precursors, respectively, dried at 50 °C for 18 h. There are a few peaks in the spectrum for the emulsion-refined powder precursor that are not present in the spectrum for the conventionally processed powder precursor, although the underlying spectra are similar, representing similar surface characteristics of the two powder precursors. The peaks at 1800, 800 and 600 cm^{-1} in the former were attributed to the residual organic traces of oil which were not effectively removed from the powder precursor during the centrifuging separation and subsequent drying at 50 °C. For verification, the emulsion-refined powder precursor was further subjected to a solvent exchange with 1,1,1 trichloroethane. A couple of distinct peaks in the range 3000–2800 cm^{-1}, which were not present in the spectrum for the conventionally processed powder precursor, were found in the spectrum for the further refined powder precursor. These peaks are believed to correspond to the vibrations of the C–H bond of methyl groups. It is apparent that the solvent exchange led to an alteration in the type of organic residuals present on the surface of the emulsion-refined powder precursor. These organic residual-related peaks subsequently

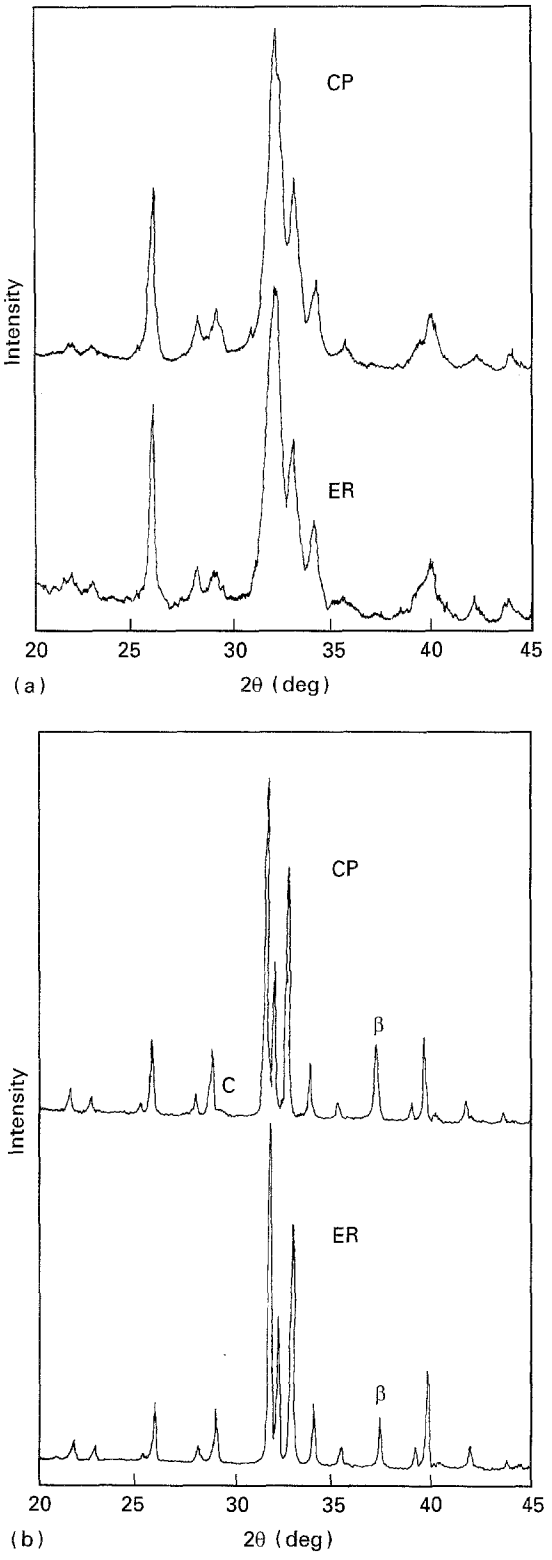

Figure 1 (a) XRD traces of the conventionally processed (CP) and emulsion-refined (ER) powder precursors dried at 50 °C for 12 h. (b) XRD traces of the sintered hydroxyapatite ceramics (1100 °C for 2 h) derived from the conventionally processed (CP) and emulsion-refined powder (ER) precursors, respectively (β: β-$Ca_3(PO_4)_2$, C: CaO).

disappeared on calcining at temperatures above 600 °C. It was, however, indicated by the FT–IR spectra that the bondings between O–H and P–O–H in the sintered hydroxyapatite processed from the emulsion-refined powder precursor were slightly different from those processed from the un-refined

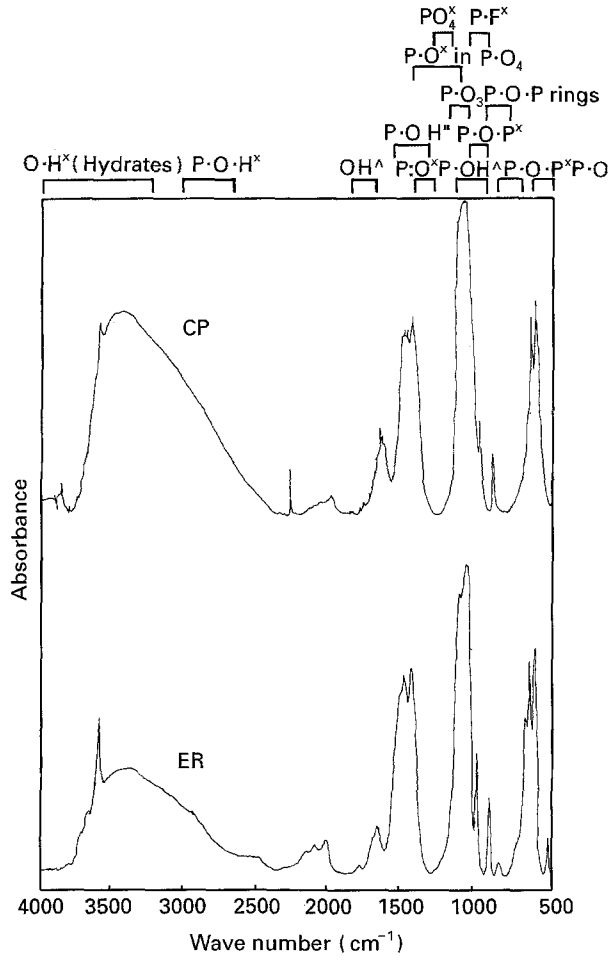

Figure 2 FT–IR spectra of the conventionally processed (CP) and emulsion-refined (ER) powder precursors dried at 50 °C for 12 h.

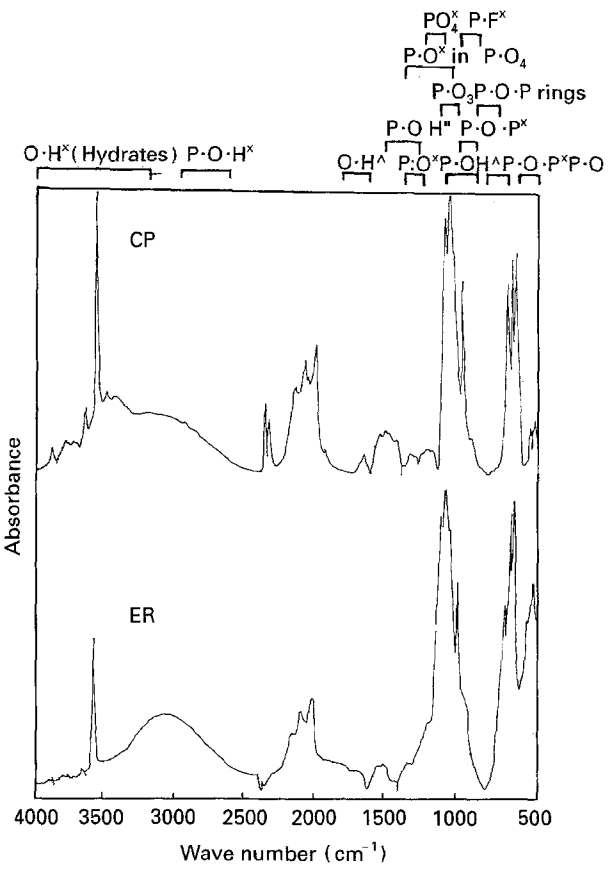

Figure 3 FT–IR spectra of the sintered hydroxyapatite ceramics (1100 °C for 2 h) derived from the conventionally processed (CP) and emulsion-refined (ER) powder precursors, respectively.

powder precursor (both were sintered at 1100 °C for 2 h), see Fig. 3a and b. The refinement had little effect on the phosphate bonding in the sintered hydroxyapatite. Further investigation of this area is needed to ascertain what the effect of this altered surface chemistry on the potential biological responses of hydroxyapatite may be.

The phase development in both the conventionally processed and emulsion-refined powder precursors with increasing temperature at a heating rate of 10 °C was monitored using both TG and DTA, Fig. 4a and b. From room temperature up to 250 °C, both powder precursors demonstrated a steady weight loss with increasing temperature due to the disappearance of free water and certain volatile organic residuals. There then follows a sharp weight loss in the emulsion-refined powder precursor, indicating that the burn-off of organic residuals such as oil is occurring over the temperature range 300–350 °C. As a result, a well-established endothermic peak, in association with the organic burn-off, is observed on the DTA trace. Little weight loss is shown in both the powder precursors over the temperature range 400–600 °C. The conventionally processed powder precursor shows a second weight loss over the temperature range 600–1000 °C, due to the elimination of certain hydroxyl groups. The exothermic peaks at > 650 °C are related to the crystallization and formation of crystalline hydroxyapatite. Similarly, the emulsion-refined powder precursor demonstrates a second weight loss over the temperature range 800–1000 °C. DTA indicates that the crystallization and formation of crystalline hydroxyapatite occur at temperatures > 820 °C. It is obvious that the emulsion refinement led to an increase in the starting temperature for crystallization of the amorphous calcium phosphate.

Another interesting difference between the conventionally processed and emulsion-refined powder precursors, found during the TG and DTA studies, is that the latter displays steeper weight loss steps over the temperature ranges 300–350 and 820–870 °C than the former, see Fig. 4a and b. Specifically, each weight loss in the latter occurs over a narrower temperature range than that in the former. Each of these weight losses is a result of eliminating a certain amount of volatile substances from the powder precursor such as water or organic residuals, a process which is facilitated by well-interconnected pore channels. The degree of powder agglomeration is, therefore, a parameter which influences the escape rate of moisture/volatile organics from the powder. The average packing density of a powder agglomerate is often higher than that of the surrounding matrix, which means less well-interconnected diffusion channels being available for the gaseous species entrapped within the agglomerates to escape. Therefore, it will take a longer period of time for the gaseous species to escape from the

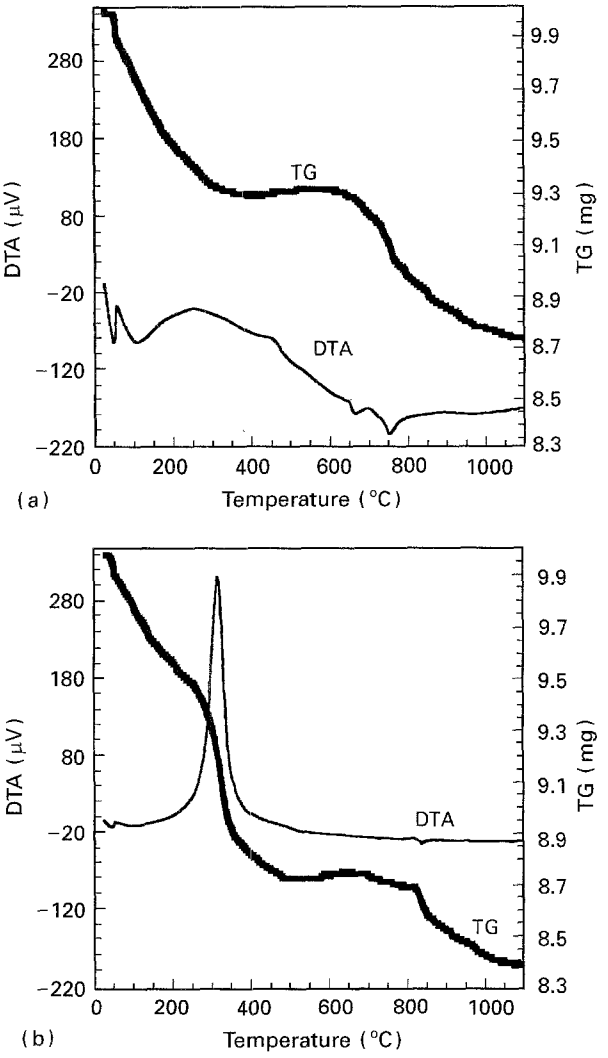

Figure 4 TG/DTA traces of (a) the conventionally processed (CP) and (b) the emulsion-refined (ER) powder precursors. Heating rate 10 °C min^{-1}.

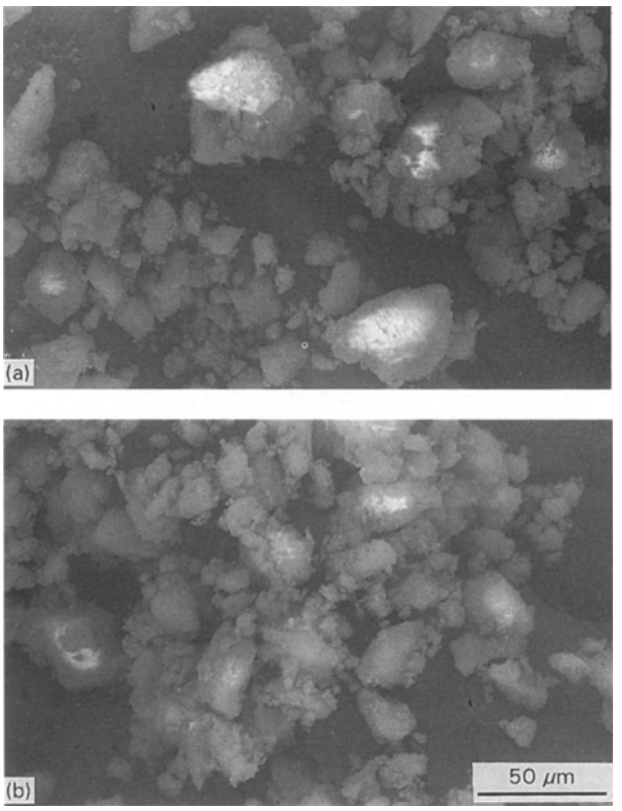

Figure 5 Scanning electron micrographs of (a) the conventionally processed (CP) and (b) the emulsion-refined (ER) powders. Both materials exhibit agglomerates of 10–50 μm in size.

agglomerates compared to that required to escape from a well dispersed powder system. At a constant heating rate (10 °C min^{-1} in the present work), the effective elimination of gaseous species from an agglomerated powder will be delayed to higher temperatures. The presence of powder agglomerates in the conventionally processed precursor was observed using SEM. Fig. 5a and b are scanning electron micrographs showing the microstructural characteristics of the two powder precursors, respectively. It can be seen that the two powder precursors are similar in both particle size and level of particle agglomeration. Agglomerates of 10–50 μm in size were observed to occur in both powder precursors. However, as will be discussed later, the emulsion refinement resulted in a "softening" of powder agglomerates. Both the strength and packing density of agglomerates in the emulsion-refined powder precursor are lower than those in the conventionally processed powder precursor. This improves the effectiveness of eliminating gaseous substances from the emulsion-refined powder precursor when it is heated during the TG/DTA studies.

3.2. Densification behaviour

The densification behaviour of the conventionally processed (CP) and emulsion-refined (ER) powder precursors was investigated in terms of (i) sintering shrinkage with rising temperature at a heating rate of 5.0 °C min^{-1} in dilatometry, and (ii) the sintering shrinkage and sintered density versus sintering temperature from 800–1100 °C (2 h at each temperature). For the dilatometry study, both powders were compacted in a steel die of 10 mm diameter at a pressure of 15 MPa. The resultant powder compacts exhibit a green density of 28.1% theoretical density (CP) and 31.6% theoretical density (ER), respectively, as determined on the basis of sample mass and dimensions. Fig. 6 shows the sintering shrinkage as a function of temperature for the two powder compacts heated at a rate of 5.0 °C min^{-1}. Little shrinkage was observed at temperatures below 400 °C for both materials. The onset temperature for noticeable shrinkage is around 400 °C for the conventionally processed powder compact, compared to 540 °C for the emulsion-refined powder compact. Over the temperature range 500–630 °C, the former exhibits a higher average shrinkage rate than that of the latter. Both powder compacts show an increase in shrinkage rate over the temperature range 630–720 °C. However, the conventionally processed powder compact demonstrates a large inflexion in sintering shrinkage over the temperature range 730–880 °C, i.e. its shrinkage rate slows down dramatically. In contrast, the emulsion-refined powder compact shows a much less apparent inflexion

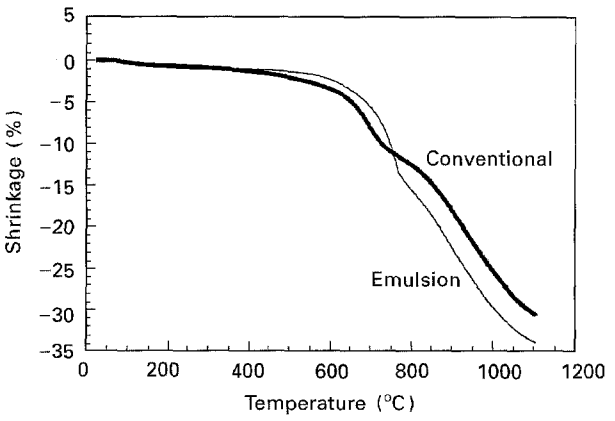

Figure 6 Dilatometry curves of the conventionally processed (CP) and emulsion-refined (ER) powder compacts from room temperature to 1100 °C. Heating rate 5 °C min^{-1}.

in sintering shrinkage over the temperature range 750–880 °C than that of the conventionally processed powder compact. The overall shrinkage of the former is, therefore, higher than that of the latter when both are heated to 780 °C. The emulsion-refined compact exhibits a total sintering shrinkage of 34.1% on heating up to 1100 °C, compared to 29.6% for the conventionally processed powder compact.

To study the sintering shrinkage and sintered density at temperatures above 800 °C, both the conventionally processed and emulsion-refined powder compacts (24 mm diameter pellets) were sintered for 2 h at 800, 900, 1000, 1100 and 1200 °C, respectively. Fig. 7a is a plot showing the sintering shrinkage as a function of sintering temperature for the two powder compacts. They exhibited a sintering shrinkage of 12.4% (CP) and 13.2% (EP), respectively, on sintering at 800 °C for 2 h. Both materials show a steady increase in the sintering shrinkage over the temperature range 800–1000 °C. However, the emulsion-refined powder compact demonstrates a surge in the sintering shrinkage from 22.9% to 39.6%, whereas the conventionally processed powder compact shows a very moderate increase from 18.9% to 25.9%, when the sintering temperature is increased from 1000 °C to 1100 °C. They both show a slight increase in the sintering shrinkage when the sintering temperature is increased from 1100 °C to 1200 °C. As illustrated in Fig. 7b, the sintered density versus sintering temperature curves almost resemble the sintering shrinkage versus sintering temperature curves shown in Fig. 7a. The emulsion-refined powder compact exhibits a slightly higher sintered density than the conventionally processed powder compact over the temperature range 800–1000 °C. However, the former demonstrates a much larger surge in the sintered density than the latter when the sintering temperature is increased from 1000 °C to 1100 °C. As a result, a much higher sintered density is observed for the emulsion refined powder compact than the conventionally processed powder compact when sintered at temperatures above 1100 °C. A sintered density of 96.32% theoretical density (TD) for the former is compared with a sintered density of 75.20% theoretical density (TD) for the latter when both are sintered at 1200 °C for 2 h.

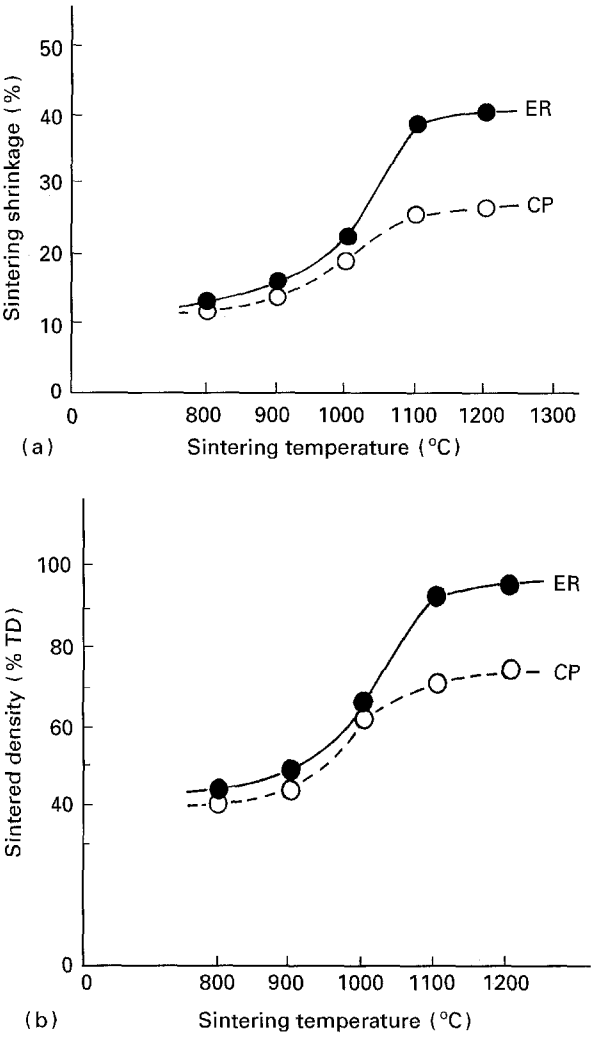

Figure 7 (a) The sintering shrinkage and (b) the sintering density, as a function of sintering temperature (2 h) from 800–1100 °C for both the conventionally processed (CP) and emulsion-refined (ER) powder compacts.

3.3. Effect of powder agglomeration on densification

As shown in Figs 6 and 7, the conventionally processed and emulsion-refined powder compacts differ in densification behaviour. The final sintered density is limited to around 75% theoretical density for the un-refined powder compact, although it exhibits a lower densification onset temperature than the emulsion-refined powder compact. In contrast, the emulsion refinement led to a sintered density of $> 96\%$ theoretical density on sintering at 1200 °C for 2 h. As discussed earlier, the aim of the emulsion-refinement step is to modify the characteristics of the conventionally processed hydroxyapatite powder precursor such as composition homogeneity and the formation of particle agglomerates. On the one hand, XRD phase analysis indicated that the emulsion refinement resulted in an increase in the crystallization temperature of amorphous calcium phosphate (this was also indicated by the DTA studies shown in Fig. 4a and b and that the emulsion-refined material was a more stoichiometrically homogeneous hydroxyapatite than the un-refined material on sintering

at 1100 °C for 2 h. However, the difference in densification behaviour between the two powder systems discussed above cannot be explained by the experimental results of XRD and DTA studies. It is believed that the emulsion refinement leads to the elimination of hard particle agglomerates from the precipitated powder precursor. The disappearance of large, hard agglomerates from the emulsion-refined powder compact resulted in an enhanced densification rate at the sintering temperature and therefore an increase in sintered density. This argument is supported by two experimental results. Firstly, the conventionally processed powder demonstrated a gradual weight loss over a wide temperature range on heating at a rate of 10 °C min^{-1}, whereas the emulsion-refined powder showed a sudden drop in weight over a narrow temperature range, as shown by the TG and DTA studies. The release of any volatile substances such as water or organic residuals from a powder system requires well-interconnected channels [20, 21]. It will be more difficult for such gaseous species to be released from an agglomerated powder than from a well-dispersed powder, due to the high packing density of the agglomerates. At a given heating rate, the effective elimination of volatile materials from an agglomerated powder will be delayed to higher temperatures [22].

Secondly, the emulsion-refined powder compact shows a higher green density (38.7% theoretical density) than the conventionally processed powder compact (33.3% theoretical density) when both are compacted in a steel die of 24 mm diameter at a pressure of 40 MPa. The improved packing density indicates that many powder agglomerates are effectively eliminated from the emulsion-refined powder compact when compacted at the pressure of 40 MPa. As shown in Fig. 5a and b, the two uncompacted powders were similar in particle and agglomerate sizes. Agglomerates of 10–50 μm in size were observed to occur in both materials. However, they differ from one another in agglomerate strength, with those in the emulsion-refined powder being weaker than those in the conventionally processed powder. A break point was seen at a pressure of 10 MPa in the density versus compaction pressure curve for the emulsion-refined powder. The discontinuity is due to the collapse of powder agglomerates [22]. Therefore, the level of particle agglomeration in the emulsion-refined powder is significantly reduced when compacted at the pressure of 40 MPa. In comparison, no such break point was seen for the conventionally processed powder over the pressure range of 0–200 MPa. The particle agglomerates in the conventionally processed powder compact therefore remain almost intact when subjected to a press pressure of 40 MPa.

To discuss the effect of powder agglomeration on the sintering behaviour and resultant microstructure of a ceramic powder compact, the powder compact considered may be modelled as consisting of uniformly sized spherical agglomerates. As shown in Fig. 8a, each powder agglomerate may be regarded as a packing unit in the agglomerated powder compact. During the initial stage of sintering, the sintering shrinkage of the agglomerated powder compact, $\Delta L/L_0$, is the sum

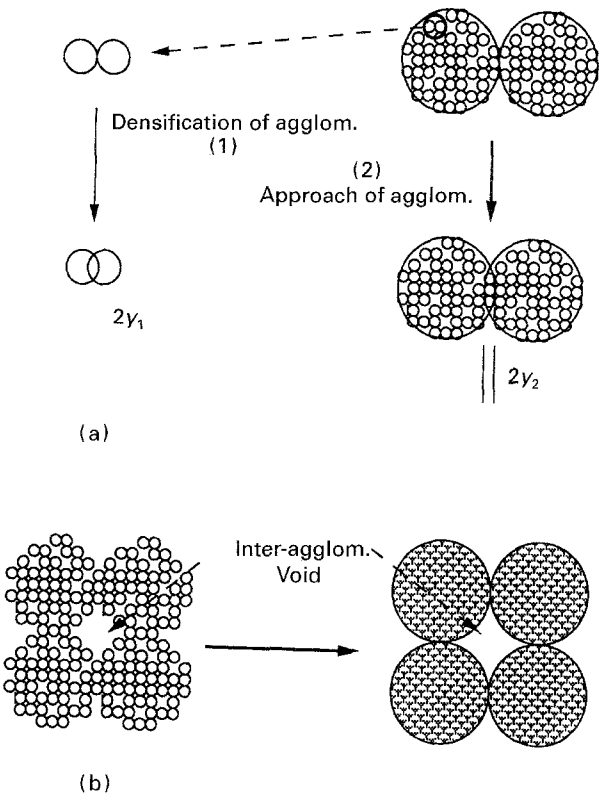

Figure 8 Schematic drawings showing the sintering of an agglomerated ceramic powder compact: (a) initial stage, and (b) intermediate and final stages.

of the relative sintering shrinkage of each powder agglomerate, $\Delta L_1/L_0$, and the relative inter-agglomerate shrinkage, $\Delta L_2/L_0$, i.e.

$$\Delta L/L_0 = \Delta L_1/L_0 + \Delta L_2/L_0 \quad (1)$$

The approach of two touching agglomerates is due to the approach of two particles in contact at the contact point between the two agglomerates. Following the analyses of Kuczynski [23] and Kingery [24], the inter-agglomerate shrinkage may be written as

$$\Delta L_2/L_0 = \frac{2y_2}{d_2} \quad (2)$$

where y_2 is the approach of two powder particles in contact at the agglomerate contact point and d_2 is the diameter of the agglomerate. Similarly, the shrinkage occurring within the powder agglomerate may be expressed as

$$\Delta L_1/L_0 = \frac{2y_1 N^{1/3}}{d_2} \quad (3)$$

where y_1 is the approach of two touching powder particles within the powder agglomerate and N is the number of powder particles contained within each powder agglomerate. y_1 and y_2 are dependent on parameters such as the sintering temperature and time, various diffusion processes contributing to densification, interfacial energy terms and the particle size [23]. Therefore, Equation 1 may be rewritten as

$$\Delta L/L_0 = \frac{2}{d_2}(N^{1/3}y_1 + y_2) \quad (4)$$

The number of the powder particles making up each agglomerate is related directly to the size of the agglomerate, thus

$$N = \rho\left(\frac{d_2}{d_1}\right)^3 \quad (5)$$

in which d_1 is the diameter of an individual powder particle, ρ is the particle packing density of the agglomerate. The total sintering shrinkage is therefore

$$\Delta L/L_0 = \frac{2}{d_2}\left[\rho^{1/3}\left(\frac{d_2}{d_1}\right)y_1 + y_2\right] \quad (6)$$

There are two extreme or limiting cases:

(i) when $d_2 \gg d_1$, i.e. the powder agglomerate is much larger than the powder particle in size, Equation 6 may be written as

$$\Delta L/L_0 = \frac{2\rho^{1/3}y_1}{d_1} \quad (7)$$

and the initial stage of sintering of the agglomerated powder compact will be dominated by the sintering behaviour of the agglomerates;

(ii) when the agglomerate size is approaching the particle size, i.e. $d_2 = d_1$, there is no shrinkage within the agglomerate, $y_1 = 0$. Equation 6 will be identical to Equation 2 ($\Delta L/L_0 = 2y_2/d_2$).

It is of interest to compare the sinterability of an agglomerated powder compact with that of an ideal agglomerate-free powder compact. As indicated by Equation 7, during the initial stage of sintering the sintering behaviour of a powder system consisting of large powder agglomerates is dictated by the sintering behaviour of individual agglomerates. In a similar situation to two powder compacts of different green density, an agglomerate with higher green density will be sintered to a required sintered density at a relatively lower sintering temperature than required by an agglomerate with lower green density [25, 26]. For a given sintering temperature and time, the former is likely to exhibit a higher sintered density than the latter. As discussed above, the particle agglomerates in the conventionally processed powder compact were not effectively eliminated by the application of a compaction pressure of 40 MPa. It may thus be concluded that the particle packing density within these hard agglomerates is higher than the average green density of the emulsion-refined powder compact, although the conventionally processed powder compact is lower in the overall green density. As has been established, an agglomerate with higher than average packing density proceeds to densification prior to the surrounding powder matrix in a ceramic powder [5, 27, 28]. At a constant heating rate, the starting temperature for densification in the former will be lower than that in the latter. Accordingly, the former will have a higher densification rate than the latter at temperatures immediately above the densification onset temperature in the former. This explains the difference in densification onset temperature and shrinkage rate shown in Fig. 6 between the conventionally and emulsion-refined powder compacts at temperatures below 630 °C, where sintering is largely limited to the initial stage.

As shown in Fig. 7a and b, over the temperature range 800–1000 °C the emulsion-refined powder compact exhibits only a slightly higher degree of densification than the conventionally processed powder compact. Above 1000 °C, the former demonstrates a larger increase in both sintering shrinkage and sintered density than the latter with increasing sintering temperature. With increasing degree of densification, the initial powder particles lose their discrete identity while the pores form a network of interconnected channels and then isolated pores lying along the grain edges [24]. During the intermediate and final stages of sintering, further densification involves the elimination of isolated pores present at the grain boundaries and grain junctions. It was during these intermediate and final stages of sintering that the sintering behaviour of the emulsion-refined powder compact departed significantly from that of the conventionally processed powder compact. The former exhibited a considerably higher sintered density than the latter when both were sintered at temperatures above 1000 °C. As an example, a sintered density of $> 96\%$ theoretical density was obtained for the former, compared to a sintered density of $< 76\%$ theoretical density for the latter when both were sintered at 1200 °C for 2 h. The presence of hard-particle agglomerates limited the occurrence of densification during the intermediate and final stages of sintering and therefore the final sintered density obtainable in the conventionally processed powder compact.

The elimination of pores from a partially densified ceramic body may be analysed using the concept of pore coordination number distribution. This thermodynamic concept, which was first introduced by Kingery and Francois [29] and further modified by Lange and Davis [30, 31], defines the pore coordination number as the number of touching grains that form the internal pore surface in a partially consolidated ceramic body. There exists a critical pore coordination number, R_c, below which a pore has the thermodynamic potential to disappear as the degree of densification increases at the sintering temperature and above which it is thermodynamically impossible for the pore to disappear although it may shrink to an equilibrium size. When the pore coordination number concept is applied to the intermediate and final stages of sintering of an agglomerated powder compact, two types of pores have to be considered. The first type are those relatively small pores which are retained within the agglomerates/aggregates and the second type are those relatively large pores which are formed at the inter-agglomerate/aggregate positions. It is apparent that the former exhibit a lower pore coordination number than the latter and it is more thermodynamically likely for the small pores to be eliminated from the partially consolidated ceramic structure than for the large pores.

The size and coordination number of the inter-agglomerate pores may be estimated on the basis of the agglomerate size and inter-agglomerate packing density. To simplify the calculation, it is assumed that the packing of the powder agglomerates takes a simple cubic structure in the as-pressed compact, and

therefore, each pore is coordinated by eight agglomerates. As shown in Fig. 8b, the coordination number of the inter-aggregate pores, R_2, may be approximated by the number of grains which cover up the agglomerate surface

$$R_2 = \pi\left(\frac{d_2}{G_f d_1}\right)^2 \quad (8)$$

where G_f is a grain growth factor, being the ratio of the grain size of the partially consolidated aggregate to the particle size of the pre-sintered powder compact. In order for the inter-agglomerate pores to be eliminated during the final stage of sintering, the pore coordination number should not be larger than the critical pore coordination number, R_c

$$R_2 \leqslant R_c \quad (9)$$

and therefore

$$d_{2c} = \left(\frac{R_c}{\pi}\right)^{1/2} G_f d_1 \quad (10)$$

This defines the largest agglomerate which can be tolerated during sintering without causing large inter-aggregate pores to form in the sintered body. For a real ceramic powder system, the critical agglomerate size or the critical number of powder particles contained within the agglomerate can be estimated on the basis of the critical pore coordination number. Most ceramic materials exhibit a dihedral angle of 100°–160°, which corresponds to a critical pore coordination number in the range 10–15 [29]. A grain growth factor in the range of 5–10 is realistic for hydroxyapatite when submicrometre-sized powders are employed as the starting materials. Bearing these figures in mind, it can be estimated that d_2 is in the range of $10–20d_1$, which implies an absolute size for the critical agglomerates in the range of 1–5 μm.

As discussed earlier, the conventionally processed powder contained a high percentage of agglomerates of 10–50 μm in size with certain agglomerates as large as > 100 μm being present. It is, therefore, thermodynamically impossible to eliminate the resultant inter-agglomerate voids, which are comparable to the agglomerates in size, unless the agglomerated structures collapse during the intermediate and final stages of sintering. To strengthen this argument, microstructural studies, using scanning electron microscopy, were carried out on the sintered hydroxyapatites derived from both the conventionally processed and emulsion-refined powder precursors. Fig. 9a–d are scanning electron micrographs showing the polished surfaces of the emulsion refined hydroxyapatite ceramics sintered for 2 h at 800, 900, 1000 and 1100 °C, respectively. All these micrographs indicate that the agglomerates of 10–50 μm in size present in the un-compacted powder (see Fig. 5) are effectively eliminated by the application of a press pressure of 40 MPa. The uniform microstructure is characterized by the narrow size distribution of pores, which are interconnected, in the partially sintered materials at 800 and 900 °C. In the material sintered at 1100 °C for 2 h, pores, which are isolated and exhibit a rounded morphology, are restricted in the range 0.1–0.4 μm in sizes although pores of 0.5–1.0 μm in size are occasionally seen. It is clearly shown that both the number of pores in a unit volume and size of each pore decrease with increasing sintering temperature, resulting in a sintered density approaching the theoretical density.

Fig. 10a–d are scanning electron micrographs showing the polished surfaces of the conventionally processed hydroxyapatite ceramics sintered for 2 h at 800, 900, 1000, 1100 °C, respectively. The microstructure at each sintering temperature is different from that shown in Fig. 9a–d. Little change was observed in both the shape and size of the inter-agglomerate/aggregate voids when the compact was sintered at temperatures below 1000 °C. However, densification occurred within the agglomerates/aggregates as indicated by the increasing density of these agglomerates/aggregates with increasing sintering temperature over the low temperature range. The inter-connected pore channels had been partially replaced by small isolated pores (0.5–1.0 μm), which exhibited a rounded morphology, when the compact was sintered at 800 °C for 2 h. Both the number of pores in a unit volume and size of each pore within the agglomerates/aggregates decreased dramatically with increasing sintering temperature from 800 °C to 1000 °C. This implies that a considerably high degree of densification was achieved within the agglomerates/aggregates when the compact was sintered at temperatures below 1000 °C. The number of pores in a unit volume and size of each pore were further reduced when the compact was sintered at temperatures above 1000 °C. As shown in Fig. 10d, the pores retained in the highly densified regions, which were hard agglomerates in the pre-sintered powder compact, are limited to < 0.5 μm. There is no doubt that many of the small pores are effectively eliminated from the agglomerates/aggregates with increasing sintering temperature. The situation is very different for the large, inter-agglomerate/aggregate pores, which are 10–50 μm in size and angular (crack-like) in morphology. They have almost retained their original sizes and shapes regardless of the increasing sintering temperature up to 1000 °C. Sintering at higher temperatures did not lead to the elimination of these large, crack-like pores, although certain intermediately sized pores (10–20 μm) were replaced by porous regions with increasing sintering temperature. Both internal sintered surfaces and inter-connected porous regions were observed to occur in the hydroxyapatite ceramic sintered at 1100 °C for 2 h. The conventionally processed hydroxyapatite ceramic sintered at 1200 °C for 2 h showed a similar microstructure. This implies that these large, crack-like pores cannot be eliminated by increasing the sintering temperature.

The microstructural studies discussed above agree well with the sintering shrinkage and sintered density, shown in Figs 6 and 7 as a function of sintering temperature. As discussed earlier, a pore has a thermodynamic potential to disappear during the intermediate and final stages of sintering if its coordination number is below a critical value. Those in the

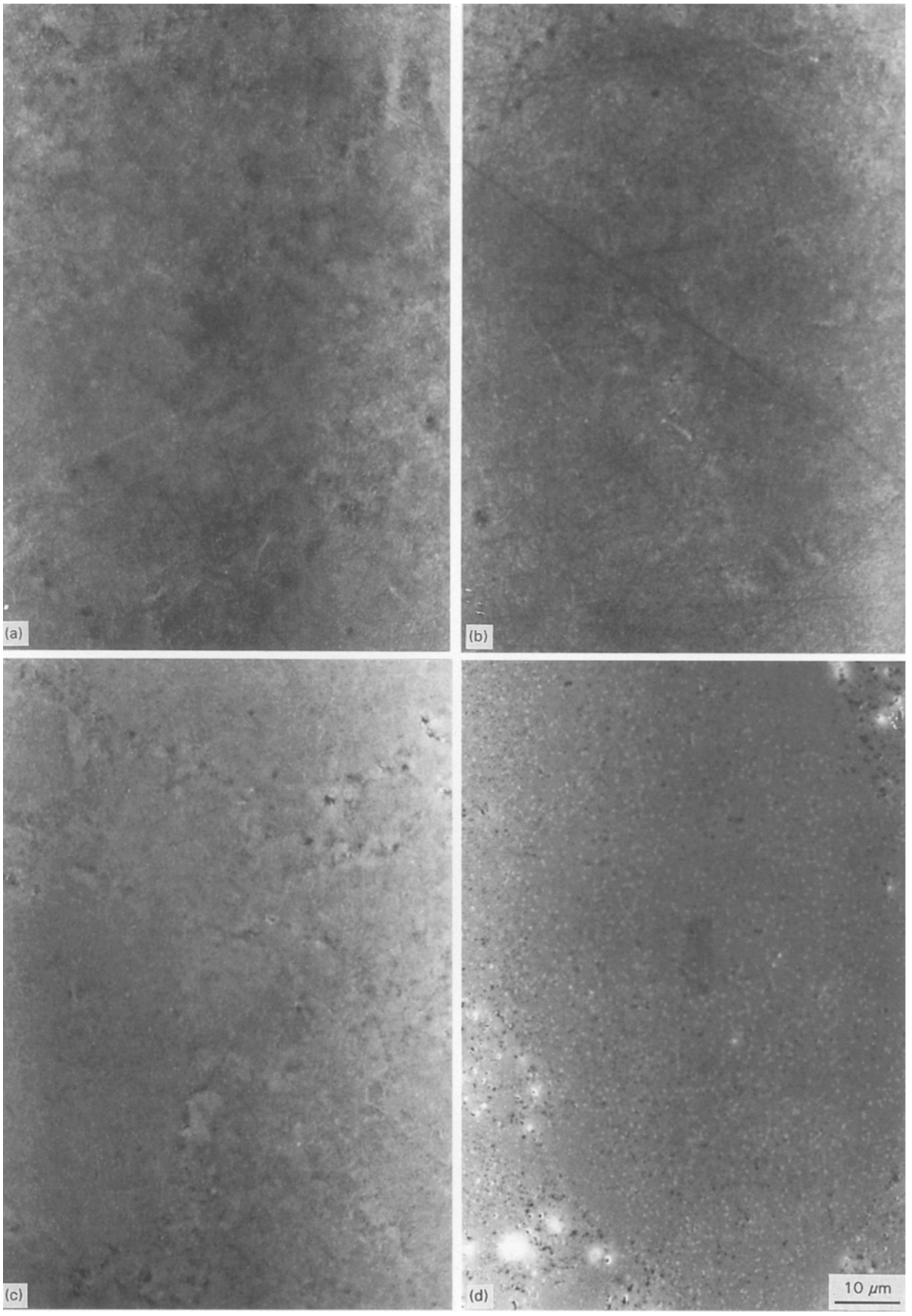

Figure 9 Scanning electron micrographs showing the polished surfaces of hydroxyapatite ceramics derived from the emulsion refined powder (ER) and sintered for 2 h at (a) 800, (b) 900, (c) 1000 and (d) 1100 °C.

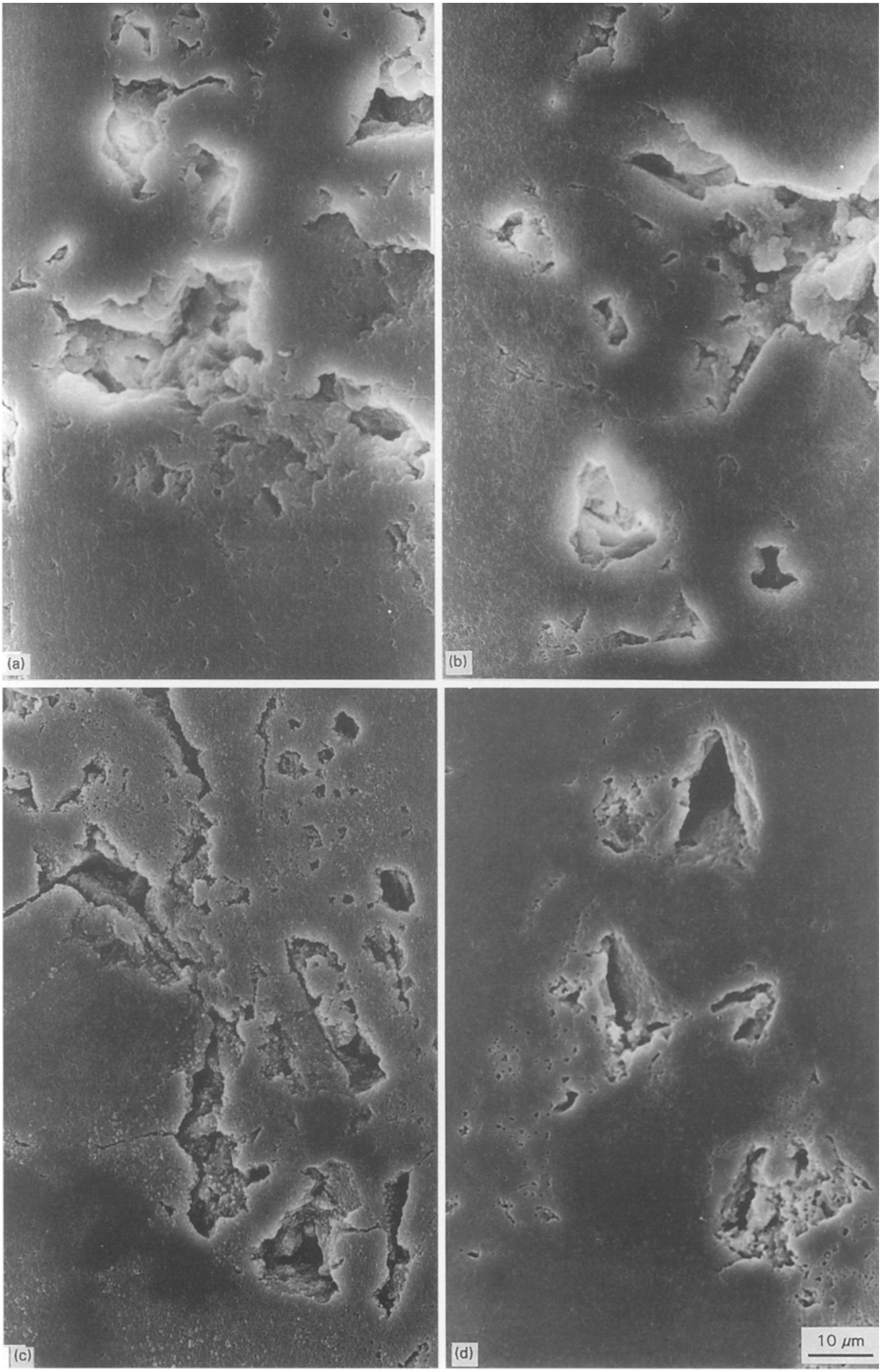

Figure 10 Scanning electron micrographs showing the polished surfaces of hydroxyapatite ceramics derived from the conventionally processed powder (CP) and sintered for 2 h at (a) 800, (b) 900, (c) 1000 and (d) 1100 °C.

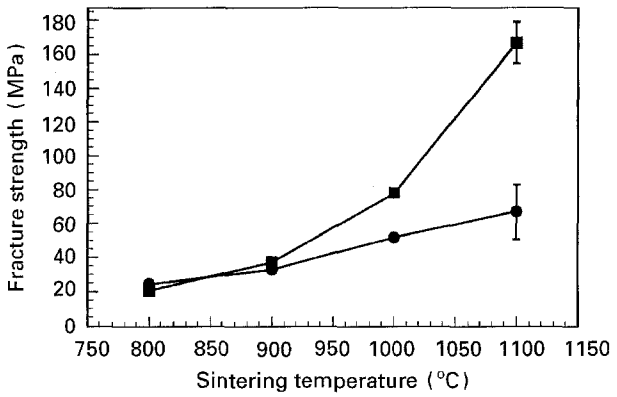

Figure 11 The fracture strength as a function of sintering temperature from 800–1100 °C for both the (●) conventionally processed and (■) emulsion-refined materials.

emulsion-refined powder compact and those within the agglomerates/aggregates in the conventionally processed powder compact belong to this category (type one). This explains the high sintered density obtained for the emulsion-refined hydroxyapatite on sintering at temperatures above 1100 °C. The attainable sintered density of the conventionally processed material is, however, limited by the presence of hard agglomerates in the pre-sintered powder compact. A network of huge voids are created at the inter-agglomerate positions, although the hard agglomerates form highly densified regions in the sintered ceramic. As a consequence of higher-than-average density, the agglomerates commence densification and reach the end-density prior to the surrounding matrix. Fig. 6 shows that the conventionally processed powder compact demonstrates an apparent inflexion in sintering shrinkage over the temperature range 730–880 °C. As indicated by the microstructural studies shown in Fig. 10a–d, the initial sintering shrinkage prior to the inflexion is largely due to the elimination of small pores within the powder agglomerates. The sintering shrinkage in the late stage, following the inflexion, involves the elimination of both small pores within the powder agglomerates and some of the relatively smaller inter-agglomerate pores. The slowdown in sintering shrinkage, seen as an inflexion, is due to the presence of large inter-agglomerate pores, which retard densification during the intermediate and late stages of sintering. The occurrence of differential sintering will further manifest both the shape and size of the existing inter-agglomerate/aggregates voids with increasing degree of sintering, resulting in the formation of large, crack-like pores in the partially sintered ceramic body [32, 33]. A pore coordination number in the range of tens to hundreds of grains is estimated for these large, crack-like pores. It is thermodynamically impossible to eliminate them during the late stage of sintering without the collapse of the agglomerated structure. Owing to the elimination of large agglomerates and, therefore, large inter-agglomerate pores, the emulsion-refined powder compact exhibits a much less-apparent inflexion in sintering shrinkage than that observed for the conventionally processed powder compact.

Fig. 8a and b assume that the agglomerated powder compact consists of uniformly sized, spherical agglomerates. This is different from the real packing structure in the conventionally processed powder compact, in which agglomerates are neither uniform in size nor spherical in shape. The wide size distribution of the powder agglomerates, see Fig. 5, is helpful in enhancing both the green density and, therefore, the sintered density. The particle/agglomerate rearrangement at the sintering temperature may also result in a decrease in the coordination number of certain inter-agglomerate pores [34]. Some of these interagglomerate/aggregate pores may eventually be replaced by porous regions in the conventionally processed material when the sintering temperature is high enough.

3.4. Mechanical properties

The increased sinterability and improved microstructure of the emulsion-refined powder compact (ER) over those of the conventionally processed material (CP) have been clearly demonstrated by the experimental results presented above. It is therefore not surprising that the sintered hydroxyapatite derived from the emulsion-refined powder precursor exhibits improved mechanical properties over that derived from the un-refined powder. Fig. 11 plots the fracture strength as a function of sintering temperature for the hydroxyapatite ceramics derived from the two powder sources. The two types of material show similar fracture strength values at each sintering temperature and their fracture strength increases slightly when the sintering temperature increases from 800 °C to 900 °C. The hydroxyapatite derived from the emulsion-refined powder precursor, however, illustrates a surge in the fracture strength from < 40 MPa to > 170 MPa when the sintering temperature increases from 900 °C to 1100 °C. In contrast, the hydroxyapatite derived from the conventionally processed powder precursor shows only a very moderate increase in the fracture strength from 35 MPa to 70 MPa when the sintering temperature undergoes the same increase. The reliability of the sintered hydroxyapatite was significantly improved by the emulsion-refinement step. As an example, the emulsion-refined hydroxyapatite exhibited a Weibull modulus of 13.5, compared to a Weibull modulus of 7.6 for the conventionally processed hydroxyapatite when both were sintered at 1100 °C for 2 h. The fracture strength of 170 MPa measured for the emulsion-refined material sintered at 1100 °C for 2 h is comparable to the highest strength value recorded for hydroxyapatite ceramics in the published work. Jarcho *et al.* [2] quoted a fracture strength of 196 MPa for one of their materials which was subjected to a long and tedious post-fabrication finishing treatment. However, a standard deviation of > 33 MPa was reported for the same material, indicating that it was not a microstructurally homogeneous material.

By correlating the above mechanical property data to the microstructural studies discussed earlier, it is apparent that the poor fracture strength of the hydroxyapatite derived from the conventionally

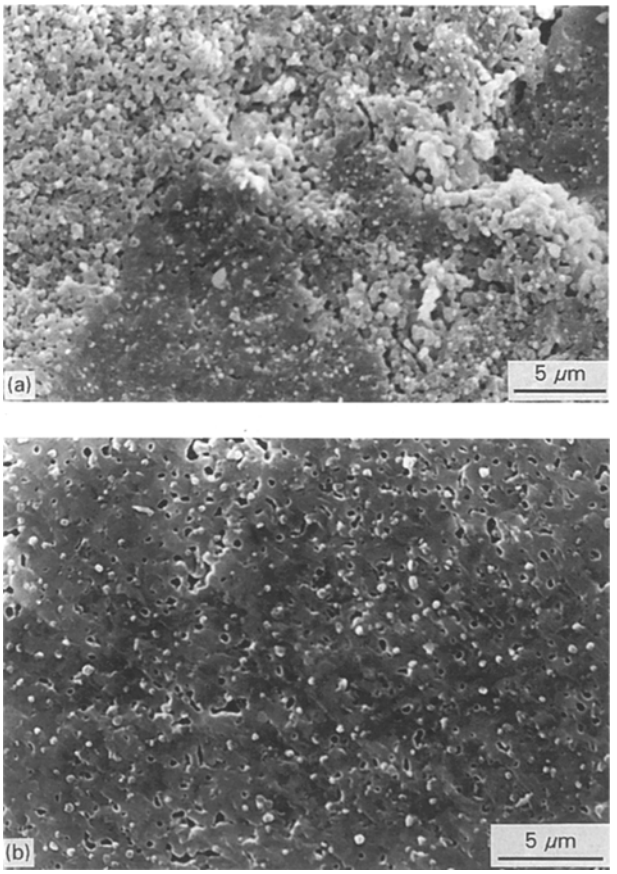

Figure 12 Scanning electron micrographs showing the fracture surfaces of sintered hydroxyapatites at 1100 °C for 2 h, derived from (a) the conventionally processed (CP) and (b) the emulsion-refined (ER) powders.

processed powder precursor is due to the presence of large, crack-like pores. It demonstrated a partially transgranular fracture surface, consisting of regions of mainly transgranularly fractured grains (highly densified regions) and regions of internal sintered surfaces (large, crack-like voids), see Fig. 12a. The size of the strength-limiting microstructural defects observed varied considerably from a few micrometres to tens of micrometres. In contrast, a primarily transgranular fracture surface was shown for the emulsion-refined hydroxyapatite, Fig. 12b, which showed a fine grain size (0.5–1.0 μm) and narrow grain-size distribution, although small rounded pores (< 1.0 μm) are present.

4. Conclusions

The conventional processing of powder precursors for hydroxyapatite ceramics, using calcium hydroxide powder and orthophosphoric acid solution as the starting materials, results in the formation of hard agglomerates. An emulsion-refinement step has proved to be effective in "softening" particle agglomerates present in the conventionally processed powder precursor. The emulsion-refined powder compact exhibits both a higher green density and a higher sintered density than the un-refined powder compact, on sintering at temperatures above 800 °C. The attainable sintered density of the conventionally processed material was limited by the presence of hard powder agglomerates, which were not effectively eliminated by the application of a press pressure of 40 MPa. These hard powder agglomerates, which form locally highly-densified regions in the sintered ceramic body, commenced densification at around 400 °C which is > 100 °C lower than the densification onset temperature for the emulsion-refined powder compact when heated at a rate of 5 °C min^{-1}. The inter-agglomerate voids, manifested by the differential sintering, resulted in the formation of large, crack-like pores, which act as the strength-limiting microstructural defects in the conventionally processed hydroxyapatite. A fracture strength of 70 MPa for the conventionally processed hydroxyapatite is compared to 170 MPa for the emulsion-refined material, when both were sintered at 1100 °C for 2 h.

Acknowledgement

The authors thank the SERC for providing financial support during the period of this work.

References

1. L. L. HENCH, *J. Am. Ceram. Soc.* **74** (1991) 1487.
2. M. JARCHO, C. H. BOLEN, M. B. THOMAS, J. BOBICK, J. K. KAY and R. H. DOREMUS, *J. Mater. Sci.* **11** (1976) 2027.
3. A. QUINTON, R. NASS and H. SCHMIDT, private communication (1994).
4. T. HATTORI and Y. IWADATE, *J. Am. Ceram. Soc.* **73** (1990) 1803.
5. F. F. LANGE, *ibid.* **72** (1989) 3.
6. J. ZHENG and J. S. REED, *Am. Ceram. Soc. Bull.* **71** (1992) 1410.
7. B. KELLETT and F. F. LANGE, *J. Am. Ceram. Soc.* **67** (1984) 369.
8. S. K. ELLIS and E. P. McNAMARA, *Am. Ceram. Soc. Bull.* **68** (1989) 988.
9. R. ROY, *J. Am. Ceram. Soc.* **52** (1969) 344.
10. A. B. HARDY, W. E. RHINE, G. GOWDA, T. J. McMOHAN, R. E. RIMAN and H. K. BOWEN, in "Ultrastructure Processing of Advanced Ceramics", edited by J. D. Mackenzie and D. R. Ulrich (Wiley, New York, 1988) p. 407.
11. B. H. ROBINSON, *Chem. Britain* (April) (1990) 342.
12. P. REYEN, H. BASTIUS and M. FIELDER, in "Ceramic Powders", edited by P. Vincenzine (Elsevier, Amsterdam, 1983) p. 499.
13. A. CELIKKAYA and M. AKINC, in "Ceramic Transactions", Vol. 1A, "Ceramic Powder Science II", edited by G. L. Messing, E. R. Fuller and H. Hausner (American Ceramic Society, Westerville, OH, 1988) pp. 110–17.
14. T. KANAI, W. E. RHINE and H. K. BOWEN, *ibid.* pp. 119–27.
15. S. D. RAMAMURTHI, Z. XU and D. A. PAYNE, *J. Am. Ceram. Soc.* **73** (1990) 2760.
16. G. H. MAHER, C. E. HUTCHINS and S. D. ROSS, *Ceram. Bull.* **72** (1993) 72.
17. S. E. FRIBERG, *Prog. Colloid. Polym. Sci.* **68** (1983) 41.
18. M. AKAO, H. AOKI and K. KATO, *J. Mater. Sci.* **16** (1981) 809.
19. S. TIMOSHENKO and S. WAINWSKY-KREIGERS, "Theory of Plates and Shells" (McGraw-Hill, New York, 1959) p. 71.
20. J. S. REED, "Introduction to Principles of Ceramic Processing" (Wiley, New York, 1989).
21. F. F. Y. WANG (ed.), "Ceramic Fabrication Processes", Treatise on Materials Science and Technology, Vol. 9 (Academic Press, London, 1976).

22. G. Y. ONODA and L. L. HENCH (eds), "Ceramic Processing Before Firing" (Wiley, New York, 1978).
23. G. C. KUCZYNSKI, *Trans. AIME* **185** (1949) 169.
24. W. D. KINGERY, H. K. BOWEN and D. R. UHLMANN, "Introduction to Ceramics" (Wiley, New York, 1976).
25. E. B. SLAMOVICH and F. F. LANGE, *J. Am. Ceram. Soc.* **73** (1990) 3368.
26. J. WANG, C. B. PONTON and P. M. MARQUIS, *ibid.* **75** (1992) 3457.
27. A. G. EVANS, *ibid.* **65** (1982) 127.
28. E. B. SLAMOVICH and F. F. LANGE, *ibid.* **75** (1992) 2498.
29. W. D. KINGERY and B. FRANCOIS, in "Sintering and Related Phenomena", edited by G. C. Kuczynski, N. A. Hooton and G. F. Gibbon (Gordon and Breach, New York, 1967) pp. 471–96.
30. F. F. LANGE and B. I. DAVIS, in "Advances in Ceramics", Vol. 12, edited by N. Claussen, M. Ruhle and A. H. Heuer (American Ceramic Society, Columbus, OH, 1984) pp. 699–713.
31. F. F. LANGE, *J. Am. Ceram. Soc.* **67** (1984) 83.
32. W. H. RHODES, *ibid.* **64** (1981) 19–22.
33. A. G. EVANS, *ibid.* **65** (1982) 497.
34. G. PETZOW and H. E. EXNER, *Z. Metallkde* **67** (1976) 611.

Received 9 August
and accepted 13 October 1994